Exploring Three-Dimensional Nanosystems with Raman Spectroscopy: Methylene Blue Adsorbed on Thiol and Sulfur Monolayers on Gold

Nicolás G. Tognalli[†] and Alejandro Fainstein*

Centro Atómico Bariloche and Instituto Balseiro, Comisión Nacional de Energía Atómica, 8400 S. C. de Bariloche, Río Negro, Argentina

Carolina Vericat, María E. Vela, and Roberto C. Salvarezza

Instituto de Investigaciones Fisicoquímicas Teóricas y Aplicadas (INIFTA), Universidad Nacional de la Plata − CONICET, Sucursal 4 Casilla de Correo 16 (1900), La Plata, Argentina

Received: August 12, 2005; In Final Form: October 31, 2005

Resonant Raman and surface-enhanced Raman scattering (SERS) spectroscopies, complemented with scanning tunnel microscopy and electrochemical techniques, have been used to obtain information about the amount and spatial distribution of methylene blue (MB) molecules immobilized on sulfur and four ultrathin molecular alkanethiolate films self-assembled on Au(111) and rough Au electrodes. The intensity of the Raman signals allow one to estimate the amount of immobilized MB at different organic films, whereas the decrease in the SERS intensity as a function of distance for the rough Au electrodes is used to locate the average position of the MB species with respect to the Au substrate. We found that significant amounts of cationic MB species are able to diffuse into methyl-terminated thiols, but they are stopped at the outer plane of the self-assembled monolayer (SAM) by negatively charged carboxylate groups. The relative shift of C−N stretching Raman modes indicates that the binding of MB to S is different from that found for MB on thiols. Most of the molecules immobilized on methyl- and carboxylate-terminated thiols are electrochemically inactive, suggesting that strong coupling between the Au electrode and the MB molecules is needed for charge transfer. Our results are consistent with a small population of electrochemically active MB species very close to the Au surface that reach this position driven by their lipophilic (hydrophobic) character through defects at SAMs.

I. Introduction

The building of metal supported molecular structures is currently one of the most active areas of research in physical chemistry because of their applications, which range from molecular electronics,[1] to biocatalysis,[2] to biosensors.[3] The so-called bottom-up technologies often involve the construction of complex structures on metallic (or semiconductor) substrates starting from simple organic molecules[4] and require a very fine control of each building step. To this end, a thorough knowledge of the physical chemistry involved is crucial. Complex molecular structures on metals are also important as biomimetic systems for understanding both the charge-transfer processes between redox-active biological species and active centers of enzymes[5] and the forces that act on the redox molecules and drive them to the exact position at which charge transfer to or from the enzyme takes place.[6]

A usual way to build these complex molecular structures involves, first, the preparation of a metal substrate covered by a strongly bonded molecular film, which acts as a spacer.[3,7] The spacer molecule can expose different chemical groups to the environment, allowing the selective anchoring of the other components of the device, such as ions, molecules, biomolecules, nanoparticles, etc.[3] Typical spacers for clean metallic substrates are self-assembled monolayers (SAMs) of thiol molecules.[8] The strong sulfur−metal bond and the hydrocarbon chain−hydrocarbon chain interactions provide robust and relatively rigid backbones.[8] The introduction of functionalized terminal groups (−COOH, −OH, −COH, $-NH_2$) allows the selective immobilization of ions, proteins, polymers, etc., either by physisorption from solutions (involving van der Waals, electrostatic, or hydrophobic forces)[3] or by covalent bonding of the ligands using specific synthetic procedures in solid or liquid phase.[2,3] The first approach is attractive due to its simplicity (avoiding complex synthetic steps) and reversibility (an interesting issue for drug release). The main disadvantage of this method is the limited control over the thickness of the adsorbed layer and the orientation of the adsorbed species.[3] In fact, the spatial location of the anchored species is uncertain due to the presence of SAM defects, such as vacancies, domain boundaries, depressions, and missing rows.[9] These defects are preferred paths that enable the diffusion of the adsorbed species, driven by repulsive molecule−solvent or attractive substrate−molecule interactions.[10] Even for covalently bonded molecules, changes in the configuration of the spacer-adsorbed species could take place to minimize the system's free energy. The determination of the amount of immobilized species and their average positions with respect to the substrate in such ultrathin spacers (usually <3 nm) are crucial points for all the above-mentioned applications. Unfortunately, the determination of these variables involves considerable difficulties. Although in principle, X-ray photon spectroscopy (XPS) and Auger electron spectroscopy (AES) can be used to determine the amount of immobilized species,[10] damage to the sample by incident or

[†] E-mail: tognalli@cab.cnea.gov.ar.
* To whom correspondence should be addressed. E-mail: afains@cab.cnea.gov.ar.

10.1021/jp054541s CCC: $33.50
Published on Web 12/10/2005

emergent electrons (or even by photons) could take place.[11] On the other hand, scanning tunnel microscopy (STM) and atomic force microscopy (AFM) allow for imaging the immobilized molecules but do not provide direct information about the position of the molecule with respect to the substrate and their possible orientations in the complex structure.

Recently, we used AES and electrochemical methods to obtain information in a model system. We have studied the immobilization of methylene blue (MB) on Au(111) by SAMs of different spacers, namely sulfur (S), propanethiol (PT), dodecanethiol (DT), 3-mercaptopropionic acid (MPA), and 11-mercaptoundecanoic acid (MUA).[10,12] MB is a positive cation in neutral and alkaline solutions similar to black nicotinamide adenine dinucleotide (NAD) and flavin adenine dinucleotide (FAD), which are redox molecules widely found in living organisms and whose main function is electron transport in different biological processes.[13] MB is also important because of its possible applications in photodynamic therapy (PDT) for the selective killing of bacteria, fungi, viruses, and cancerous cells.[14−17] In fact, polyacrylamide nanoparticles loaded with MB have been designed to be administered to tumor cells externally and to deliver singlet oxygen ($^1O_2$) for killing cells via oxidative stress to the membrane.[14] High uptake of MB in cancerous cell cultures has been observed.[15] MB aggregation on the surface of Qβacteriophage has also been observed, the amount of MB being dependent on the ionic strength.[16] It has been also shown that MB adsorbs on cholesterol surfaces.[17] However, as discussed in ref 18, the origin of the interaction forces of living cells with a variety of stains remains obscure.

In previous studies,[10,12] and on the basis of indirect voltammetric data, we have proposed that, for carboxylate-terminated thiols, MB molecules are mainly at the outer plane of the SAMs, "trapped" by electrostatic interactions. On the other hand, also on the basis of the electrochemical behavior of the system, some penetration of the MB molecules into the SAMs has been suggested for methyl-terminated SAMs. Moreover, from AES data, we have shown that the carboxylate-terminated thiols "trap" MB ions more efficiently than methyl-terminated thiols.[10] However, this ultrahigh vacuum (UHV) technique has been unable to detect MB "trapped" in propanethiolate SAMs, in contrast to voltammetry, which does indicate the presence of a small amount of immobilized species for this thiol. One can speculate that either the amount of MB is below the AES detection limit or loss of material takes place in UHV under irradiation.

It is evident that other techniques are needed to make a complete description of this molecular system. In fact, the correlation between the amount, distance to the substrate, and electrochemical activity of immobilized species in three-dimensional nanosystems is a key point for the understanding of charge transfer in biomimetic systems and also for the development of efficient biosensors and electronic devices based on organic molecules.

Raman spectroscopy is a powerful tool for exploring this type of nanosystem. First, it is highly specific through the vibrational spectra that can be used as a fingerprint of the immobilized molecule. Second, when electronic resonant (RRS) or plasmon resonant surface enhancement (SERS) is possible, Raman scattering can be sensitive down to fractions of monolayers[19,20] or even to single molecules.[21−23] Third, when vibrational mode energy shifts or changes in the relative intensities of Raman peaks are present, they provide information on the molecular orientation and binding.[24,25] Usually this information is qualitative, being a more precise determination possible when microscopic models of the molecular vibrational modes or Raman tensors are available. And finally, through the strong metal−molecule distance dependence of the SERS enhancement, important insight into the relative location of molecules with respect to the metal can be obtained.[26,27] Such kinds of studies are, however, limited when sample reproducibility is an issue.

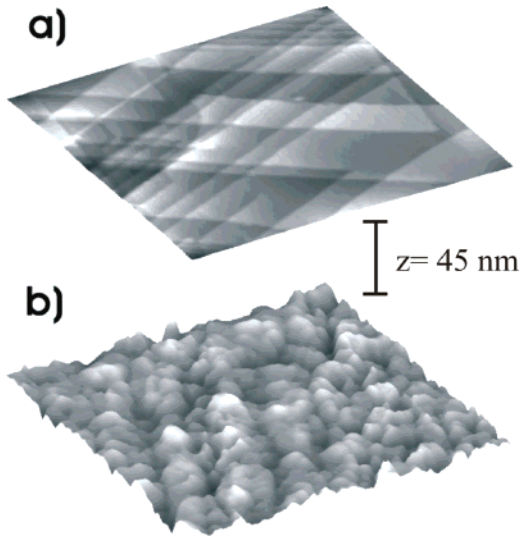

Figure 1. 230 × 230 nm^2 STM images of (a) a Au(111) electrode and (b) a rough Au electrode. The *z* range for both images is 45 nm.

In this work, we have used resonant Raman and SERS spectroscopies, complemented with STM and electrochemical techniques, to obtain information not only on the amount but also on the spatial distribution of MB molecules immobilized on different spacers on Au(111) and rough Au electrodes. The intensity of the Raman signals allows us to estimate the amount of immobilized MB for the different spacers, that is, S, PT, DT, MPA, and MUA. The attenuation of the SERS intensity with distance for the rough Au electrodes is used to locate the average position of the MB molecules in the SAM-covered systems. Changes in the Raman spectra, on the other hand, are analyzed in terms of possible binding configurations. The electrochemical data together with the determined molecule−substrate distance give information about the charge-transfer process taking place between the substrate and the immobilized molecules.

II. Samples and Experimental Set-Up

We have performed experiments with MB immobilized on both atomically flat Au(111) and nano-/microstructured rough Au substrates modified by SAMs of different spacers: S, methyl-terminated (PT and DT), and carboxylate-terminated (MPA and MUA) thiol SAMs. The pairs PT/MPA and DT/MUA have basically a similar structure and length and differ only in their termination group (nonpolar in the case of methyl and polar in the case of carboxylate). Before self-assembly, the flat Au(111) thin films evaporated on glass (AF 45 Berliner Glass KG, Germany) were annealed for 5 min in a butane−propane flame until the film color turned to a dark red. As observed by STM and AFM,[28] these Au electrodes exhibit atomically smooth (111) terraces with monatomic steps (Figure 1a). Rough Au substrates (SERS-active) were prepared by the electrochemical roughening procedure described in ref 29. Briefly, a thick hydrous Au oxide film is formed by anodization of Au at a relatively high applied potential, followed by voltammetric electroreduction. Au foils, 99.99% pure, were immersed in a 0.5 M H_2SO_4 solution and held for 10 min at

2.4 V (vs a Ag/AgCl reference electrode). Finally, the potential was scanned down to −0.6 V at a rate of 0.02 V/s. The surface of the resulting electrodes consists of Au nano-/microparticles with sizes ranging from 20 to 200 nm, as shown in Figure 1b. The surface area of the electrodes was calculated by measuring the AuO monolayer electroreduction charge (q), considering that one monolayer involves 0.42 mC cm^{-2}.[29]

Concerning the SAMs assembly, the solutions were prepared by using analytical-grade chemicals and Milli-Q water. First, the Au substrates were immersed in 0.1 mM PT, DT, MPA, and MUA ethanolic solutions for 24 h to form the corresponding SAMs.[3−6] In the case of S, the Au substrates were immersed in 3 mM Na_2S aqueous solutions saturated with nitrogen for 15 min. Under these conditions, the well-known S_8 structures are spontaneously formed on Au electrodes, as described in ref 30.

The thiol-covered substrates were rinsed with ethanol and then with water; the S-covered substrates were rinsed only with water. To test the spacer density for both electrodes, we have estimated the electrodesorption charge of the S and thiol molecules from both the Au(111) and rough Au surfaces, finding the same charge densities: 0.15 mC cm^{-2} for S and 0.08 mC cm^{-2} for thiols, irrespective of the substrate surface structure. These charge density values are those expected for complete S_8 and thiols monolayers on Au substrates.[30,31]

Immobilization of MB species on the spacer-modified Au substrates was performed by immersion for 30 min in freshly prepared 0.1 mM MB + 0.1 M NaOH aqueous solutions.[10,12] Samples were rinsed with water and dried with a N_2 gas flow. The Raman experiments were performed using a Jobin-Yvon T64000 triple spectrometer operating in subtractive mode and equipped with a liquid-N_2-cooled charge-coupled device. The excitation was performed with an Ar−Kr ion laser using energies between 1.834 eV (673 nm) and 2.707 eV (458 nm). Typical powers were around 10 mW, concentrated on either a ∼100-μm-diameter circular spot or a 7 mm long and ∼100 μm wide line focus. These were chosen to reduce the photon-induced degradation of the samples. Under the worst situation (circular spot) the photobleaching was determined to be around 5% after 15 s of data acquisition. To avoid accumulating this effect, a fresh spot in the sample was used after taking each spectrum. Prior to this, a Raman map of the samples was performed with very low powers and acquisition times to exclude spots displaying Raman intensities very different from the average value. For the resonant Raman scans, the Raman intensity was corrected for the setup response.

To check for repeatability, several complete series of measurements were performed for MB immobilized on SAMs assembled with the five different spacers and using the two kinds of substrates.

Results and Discussion

To characterize the resonant Raman response of the immobilized MB structures, resonant Raman scans were performed for the different spacer structures both on Au(111) and on rough Au substrates. Basically, the same behavior was observed for MB on S and on the various thiols. This behavior is illustrated in Figure 2 for the case of MB−S. In the inset, a typical Raman spectrum is shown, corresponding to the molecular vibrations of MB. The shown spectrum was collected on the rough substrate with 3 s acquisition time. It illustrates the large Raman signal-to-noise ratio accessible with submonolayer MB coverage. Some specific modes which were used to determine the resonant Raman behavior (Figure 2) and in the following discussion are indicated. These modes have been assigned to a C−N−C skeleton bending (443 cm^{-1}, labeled with a tilted square), C−N symmetric stretching (1387 cm^{-1}, circle) and C−C ring stretching (1610 cm^{-1}, square), respectively.[32,33] The intensities of these modes as a function of laser energy are displayed in Figure 2 for the flat Au(111) substrate (top panel) and for the roughened SERS active electrode (bottom panel). The maximum Raman intensity of the different modes has been normalized, for the Au(111) grown structure, to 1. For the rough electrode, on the other hand, the normalized maxima of the curves are given relative to the Au(111) maximum enhancement.

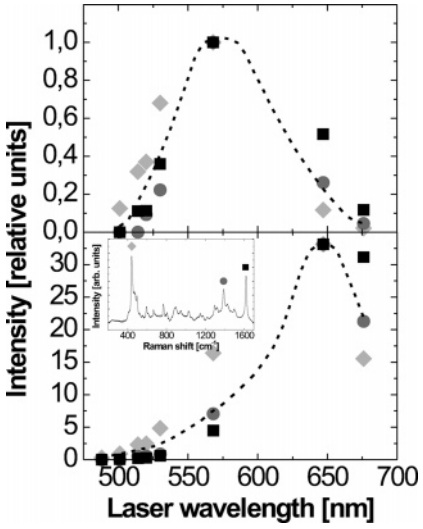

Figure 2. Inset: typical Raman spectra corresponding to the molecular vibrations of MB. Some specific modes which were used for the characterization to be presented in this and in following figures (see text for details) are indicated. The figure presents resonant Raman scans as a function of laser energy, performed for the S spacer both on Au(111) (top) and rough Au (bottom panel) substrates. The different labels indicate Raman intensities derived from the various Raman lines labeled in the inset. Note the shift of the resonance from ∼568 nm for flat Au(111) to ∼650 nm for the rough Au electrode, evidencing the evolution from electronic resonance to SERS amplification of the Raman process.

Two main features should be highlighted in Figure 2: (i) The maximum of the resonant Raman scans falls at different energies for the two substrates, namely, ∼568 nm for flat Au(111) and ∼650 nm for rough Au. These correspond, respectively, to the electronic resonance of MB and to the rough electrode plasmon energy. The latter signals the presence of SERS enhancement. (ii) The maximum intensity observed on the rough Au substrate is ∼30 times larger than that amplified through an electronic resonant mechanism. Considering that at 650 nm, the normalized Raman intensity on Au(111) is ∼0.2, this implies a SERS amplification on the rough Au electrode of ∼150. As will be discussed below, the variation of this SERS enhancement for the different studied spacers can be used as an indication of the MB average distance to the substrate and, consequently, of the location of the MB molecules when immobilized.

As commented in the Introduction, previous studies of MB on different SAMs used either electrochemistry or AES to determine the amount of immobilized MB.[10,12] Voltammetric cycles provide a rather indirect measure of this quantity, because adsorbed MB molecules may not be electrically wired to the substrate. On the other hand, AES is limited both by the damage that it induces on the molecular structures and by the small (and difficult to quantify) penetration depth of electrons. In contrast, in Raman scattering, light penetrates through all the structure, it can be focused in microscopically small spots (typically

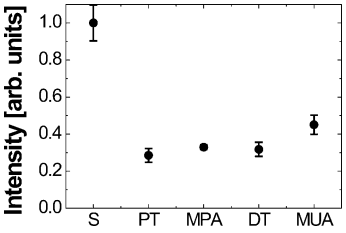

Figure 3. Raman intensity, corresponding to the 1610 cm^{-1} C−C ring stretching vibration labeled with a square in Figure 2, for MB immobilized with the five studied spacers (S, PT, MPA, DT, and MUA). The Raman measurements were taken on flat Au(111) under electronic resonance conditions with the yellow line of the Ar−Kr laser (568 nm, see the top panel of Figure 2). The displayed Raman intensity is the result of averaging four complete series of measurements, each series involving the five SAMs and data collected on 20 different spots on each sample.

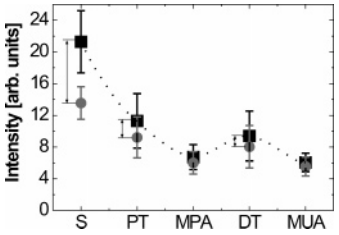

Figure 4. Raman intensity (corresponding to the 1610 cm^{-1} C−C ring stretching mode) collected with both the preresonant yellow laser line (568 nm, indicated with circles) and the fully SERS-resonant red line (647 nm, indicated with squares) on samples grown with the five different spacers on rough, SERS-active Au electrodes. To make the measurements independent of the MB mass present in the samples, the measured yellow and red laser line Raman signals were divided by the Raman intensity determined using the off-resonant green 514.5 nm laser line (see Figure 2, bottom panel). The arrows highlight the differences between the fully resonant (red) and the partially resonant (yellow) laser signals for the different spacers.

limited by diffraction down to $\sim 1\ \mu$m), and it generates reduced and measurable damage. To evaluate the amount of MB immobilized with the various spacers, resonant Raman measurements were taken on Au(111) using the electronic resonant yellow line of the Ar−Kr laser (568 nm, see the top panel of Figure 2). For this study, Au(111) was chosen (not rough Au) because it has been much better characterized and also because of the expected lower density of defects in the assembled monolayers. It is to be noted, however, that basically the same trend is observed for the SAMs grown on the rough Au electrodes. For the rough substrates, the excitation was performed at 514.5 nm, that is, out of SERS amplification. As we will argue below, when SERS is also present, the intensity is dependent not only on the mass coverage but also on the specific spatial distribution of the molecules. The Raman intensity corresponding to the well-separated 1610 cm^{-1} C−C ring stretching vibration, labeled with a square in Figure 2, is displayed in Figure 3 for MB molecules immobilized on Au(111) with the five studied spacers.

Figure 3 resumes the results of four complete series of measurements. A single series consisted of typically 20 spectra taken on different spots of each one of the five samples having the different studied spacers. The displayed Raman intensity for each spacer was obtained as a weighted average of the data collected on the four independent series. This intensity can be taken as a direct measure of the amount of MB present in the samples.[19] The main conclusions can be summarized as follows: (i) S is the most efficient SAM for MB immobilization, with a MB surface concentration 2−3 times larger than for the thiol covered substrates. Essentially the same behavior was observed in complementary XPS measurements of N and S concentration performed on one of the series of samples used for the Raman scattering study (data not shown). (ii) All thiol spacers display basically the same amount of MB. Notwithstanding this general tendency, we have systematically observed larger MB Raman signals on the carboxylate-terminated thiols (MPA and MUA), as compared to their methyl-terminated counterpart (PT and DT). In fact, there is a decrease in the efficiency of MB immobilization when going from S to carboxylate thiols and, finally, to methyl-terminated thiols. This confirms our previous observation[10] that carboxylate-terminated SAMs are more efficient to immobilize MB molecules than methyl-terminated SAMs due to electrostatic interactions. However, and more interesting, we have been able to detect a significant amount of MB immobilized in methyl-terminated alkanethiols, in contrast to our previous results from AES. This suggests that MB-hydrocarbon chain interactions are weaker than the electrostatic interactions at carboxylate-terminated alkanethiols so that the electrons involved in the Auger process may easily desorb MB from the methyl-terminated SAMs.

In addition to providing a rapid and precise determination of MB mass content, Raman experiments performed on the rough SERS-active Au substrates can be used to provide information on the MB−SAM structure. In fact, the strong dependence of SERS amplification on the distance between the molecule and the active metallic substrate can be used to extract information on the molecule localization in space.[26,27] Figure 4 presents the Raman intensity (corresponding to the 1610 cm^{-1} C−C ring stretching mode) for samples grown with the five different spacers on rough Au, collected with both the yellow laser line (568 nm, indicated with circles) and the red line (647 nm, indicated with squares). These two laser lines correspond, respectively, to a SERS preresonant and a fully SERS-resonant condition as follows from Figure 2 (bottom). The Raman intensity is determined both by the molecular concentration and by the distance between molecule and substrate. To make the measurements independent of the MB mass present in the samples, the measured yellow and red laser line Raman signals were divided by the Raman intensity determined using the off-resonant green 514.5 nm laser line (see Figure 2, bottom panel). The latter, not influenced by SERS enhancement, can be taken as proportional to the MB molecular content of the assembled structures. As commented above, the MB mass concentration in the rough electrodes determined through these off-resonant experiments basically reproduces the trend observed for the flat Au(111) samples in Figure 3.

The results displayed in Figure 4 clearly establish that SERS enhancement is larger for S, followed by PT and DT, and smallest in the carboxylate-terminated MPA and MUA. In fact, the decreasing difference observed along this sequence between the fully resonant red and partially resonant yellow laser signals (indicated with arrows in Figure 4) is a check of consistency of the above conclusion. In addition, because for MPA and MUA the 568 and 647 nm Raman intensities are very close, it indicates that SERS is comparatively weaker for the carboxylate-terminated thiols. On the other hand, although the difference is small and within experimental error, we have systematically observed, as illustrated by Figure 4, that the SERS enhanced Raman intensities are slightly larger for PT than for DT. In view of the fact that SERS enhancement decreases with the separation between the Raman active molecule and the metallic substrate, we conclude from this study that the average distance of MB to the substrate surface is the smallest for the S spacer, followed by PT and DT, and is largest for MPA and MUA. On the basis

TABLE 1: SAMs' Nominal Thickness, Average MB−Au Distances, and Amount of MB[a] Derived from Raman Measurements and Charge Densities (q_{MB}) and Heterogeneous Rate Constants (k) Measured by Voltammetry for the Five Studied Spacers

spacer	SAM thickness[b], Å	av MB−Au distance(s), Å	amt of MB, monolayers	q_{MB} μcm^{-2}	k[c], s^{-1}
S	2	∼2	1	50	12−18
PT	5.2	∼6	≤0.3	2−4	120−260
DT	15	∼8	∼0.3	2−4	35−60
MPA	5.4	∼10	∼0.3	2−4	10−30
MUA	14.1	∼12	∼0.45	2−4	5−9

[a] Referred to a MB−S complete monolayer. [b] Estimated from the molecular length and a 30° tilt with respect to the substrate normal. [c] Taken from ref 10.

of models and published experimental results on SERS enhancement decay with distance,[26,27] one may estimate the average separation between the MB molecules and the metal surface. These values are given in Table 1. Even allowing for the clear uncertainty of such estimations, it is possible to conclude that MB penetration into the DT spacer is large, but a partial diffusion into the longer chain MUA spacer cannot be discarded. All this qualitative and semiquantitative evidence provides a structural picture of MB immobilized through the different spacers on Au substrates. Such a picture is schematized in Figure 5.

All the reported results are consistent with a model in which (a) MB forms a dense monolayer on S close to the Au surface; (b) for PT and DT, MB is bonded by van der Waals and hydrophobic forces within defects between the thiol chains; and (c) in MPA and MUA, MB is kept further away from the surface than in the case of their methyl-terminated counterparts due to electrostatic interactions. Our picture about methylene blue behavior in the SAMs is consistent with that expected for amphipathic, lipophilic cations with moderately sized conjugated systems routinely used as stains to visualize the endoplasmic reticulum in living cells. The moderately lipophilic character permits probe uptake by passive diffusion without nonspecific accumulation in biomembranes (MB in PT, DT). The moderately amphipathic character favors uptake into the endoplasmic reticulum, perhaps owing to its high concentration of zwitterionic lipid headgroups (MB in MPA, MUA).[16]

Further insight onto the bonding mechanism may be obtained by an analysis of the MB Raman spectra on the different structures. Raman peak shifts and changes of relative intensities are signatures of additional interactions and varying molecular orientations or environments. We have not observed any clear difference in the Raman spectra of MB below 1200 cm^{-1}, where modes involving S may be expected. In particular, the Raman peak at 405 cm^{-1}, assigned in ref 33 to a C−S−C bending mode, remains unaltered for MB on the five spacers. The same occurs for several peaks observed in the spectra between 1100 and 1200 cm^{-1} and around 550 cm^{-1}, which, according to our semiempirical calculations using the AM1 model,[34] involve C−S bond stretching. On the other hand, as shown in Figure 6 for spectra taken using the 568 nm line, clear changes occur that involve C−N displacements. In fact, we have systematically observed that the C−N asymmetric vibration, observed for MB on PT, DT, MPA, and MUA at 1424 cm^{-1}, clearly shifts down to 1412 cm^{-1} when MB is immobilized on S. These results provide strong evidence that MB bonds to S-modified Au through one or both of the dimethylamino groups, as suggested by Campbell et al.,[35] and not through a sulfur−sulfur interaction.[36] We note, in addition, that in the same spectral region there is another peak (shadowed in Figure 6) that is clearly present for MB on S, PT, and DT, but that appears at most as a weak shoulder for the carboxylate-terminated thiols MPA and MUA. This result may be reflecting a selection rule-induced intensity variation,[24] indicating that the orientation of the MB molecule is similar in S, PT, and DT and different from that in MPA and MUA. To the best of our knowledge, however, this peak has not been unambiguously assigned in the literature. In fact, the full use of such potentially rich data is usually complicated by the ambiguous assignments of vibrational modes and the lack of knowledge of relevant Raman tensors. The theoretical evaluation of the latter requires a detailed microscopic calculation of electronic and vibrational properties of the molecules, an approach that is beyond the scope of this paper.

Other information about the nature of the immobilized MB species can be obtained from the Raman spectra, shown in part a of Figure 7, and STM images, as displayed in parts b and c. In the case of MB adsorbed on rough Ag,[37] the signal at 480 cm^{-1} has been assigned to thiazine ring in-plane bending of MB adsorbed as a monomer. According to ref 37, its intensity relative to that of the signals at 440 and 495 cm^{-1} can be used to quantify the concentration of MB monomers relative to dimers or aggregates adsorbed on Ag. In our case, the signal at 470 cm^{-1} is rather small, suggesting that only a small fraction of MB is under the form of monomers. Such an aggregation of MB molecules is, furthermore, consistent with STM images of the studied samples. STM images of MB on MPA and on S assembled on Au(111) are shown in Figure 7b and c, respectively. In the case of MB on MPA, the surface is randomly covered by bright ∼2 nm spots that are somewhat bigger than the size of a single MB molecule lying down or parallel to the substrate surface (∼1 nm). As follows from Figure 7c, the

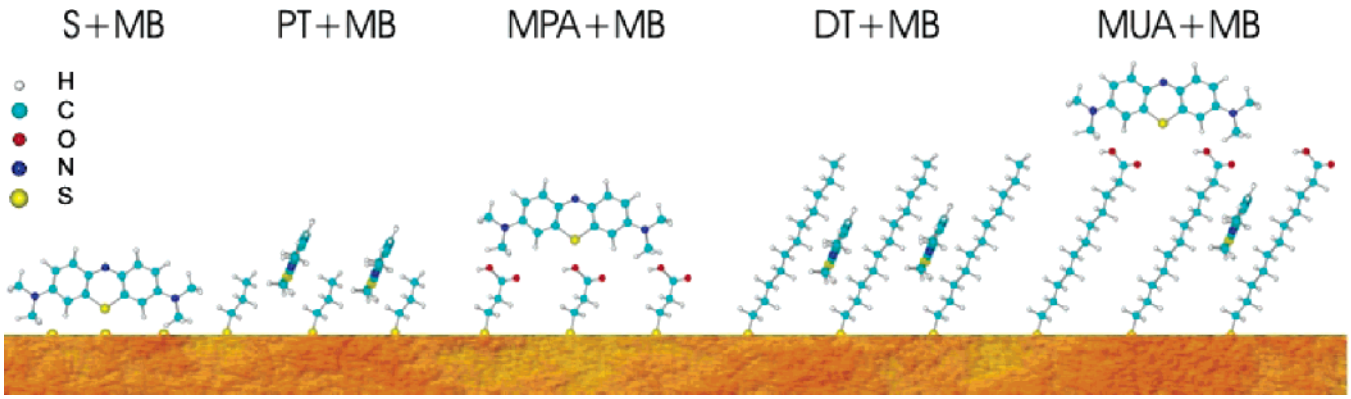

Figure 5. Scheme showing the *average* position of MB immobilized by the different spacers on Au, as concluded from the Raman results reported here.

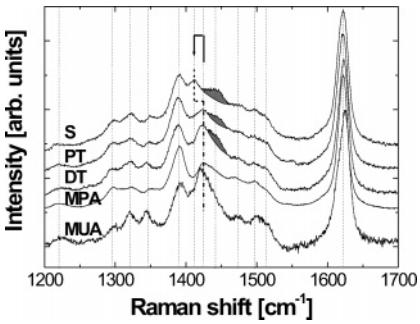

Figure 6. Raman spectra of MB immobilized by the different spacers on rough Au. The spectra were taken with the 568 nm line of the Ar−Kr laser. Note the clear shift of the MB C−N asymmetric vibration, which is observed at 1424 cm^{-1} for MB on the four thiol spacers and at 1412 cm^{-1} when MB is immobilized on S. A peak observed at 1442 cm^{-1} for MB on S, PT, and DT (and not for MPA and MUA) is highlighted. The vertical lines are guides to the eye to indicate the position of the Raman peaks.

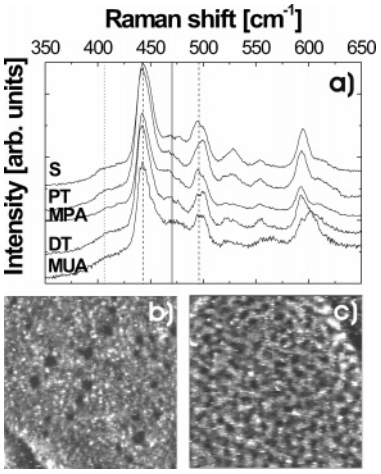

Figure 7. (a) Raman spectra of MB adsorbed on the five different spacers taken with the 568 nm line of the Ar−Kr laser. The 470 cm^{-1} peak (full line) is rather small when compared with those at 440 and 495 cm^{-1} (dashed lines), suggesting that only a small fraction of MB is under the form of monomers. The small peak at 405 cm^{-1} (dotted line) assigned to C−S−C ring bending does not show differences between the spacers. STM images (70 × 70 nm^2) of (b) MPA−MB-covered Au(111) (E_{bias} = 600 mV, I_{tunnel} = 800 pA) and (c) S−MB-covered Au(111) (E_{bias} = 500 mV, I_{tunnel} = 605 pA). The gray scale represents changes in height between 0 nm (black) and 1 nm (white).

density of spots is higher for MB on S than for MB on MPA. This suggests the presence of larger aggregates,[37] which in turn is consistent with the increased amount of immobilized MB on S, as determined by Raman scattering and presented in Table 1. Note that the MB solutions used in this work contain both the dimer and the monomer MB species.[38] Therefore, if the assignment of the peak at 470 cm^{-1} made in ref 37 is correct, it is evident that the scheme shown in Figure 5 should be improved, showing MB aggregates rather than only MB monomers. In any case, the interactions with the spacer would be pretty much the same.

In what follows, we correlate the model depicted in Figure 5 with data about the charge-transfer process in these systems. Figure 8 shows typical voltammograms recorded at 0.5 V s^{-1} for the MB redox couple immobilized on the different spacers. The voltammograms show broad peaks, those corresponding to MB on PT and DT being the most reversible, followed by those of MB on MPA and MUA. On the contrary, MB on S exhibits a higher degree of irreversibility. Note that the cathodic charge density (q_{MB}) observed for MB on S is larger than that

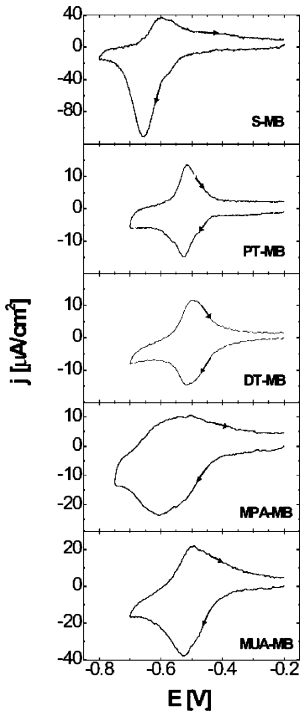

Figure 8. Voltammograms for MB immobilized on different SAM-covered Au(111) electrodes after immersion (dipping) in 0.1 mM MB + 0.1 M NaOH for 30 min. Electrolyte solution: 0.1 M NaOH. υ = 0.5 V s^{-1}.

observed in the anodic scan, indicating that reduced MB species go to the solution.[35] Conversely, the fact that the charge density remains practically unchanged for MB on PT and DT is a clear indication that the MB molecules are trapped inside the SAMs. An intermediate behavior can be observed in the voltammograms corresponding to MB on MPA and MUA, supporting the previously obtained results that indicate that MB on carboxilic ended thiols can bind both, outside or inside the SAMs. The q_{MB} values involved in the voltammetric cathodic peaks are a direct measure of the number of MB molecules that are able to participate in the charge-transfer process. Voltammetry also allows a rough estimation of the heterogeneous rate constant for electron transfer.[1,39] In Table 1, we show the SAMs' nominal thickness, the average MB−Au distances and the amount of MB (referred to an MB−S complete monolayer) derived from the Raman measurements, and the charge densities (q_{MB}) and heterogeneous rate constants (k) measured by voltammetry (from ref 10) for the studied systems.

It is evident that in all cases, q_{MB} for MB immobilized on S is 10 times greater than that observed for MB immobilized on the thiol spacers. This factor is larger than the 3−2 factor observed from Raman measurements, thus confirming that a large number of immobilized redox species are not electrochemically active for thiol spacers. Some information can also be obtained by considering the k values (taken from ref 10) shown in Table 1. As expected, in the case of MB immobilized in thiol spacers, k decreases with increasing MB−substrate distance (s, estimated from the SERS data). However, the decay of k with s is much smaller than $d \ln k/ds \cong \beta \cong .9-1.0$ $Å^{-1}$ observed for other immobilized redox species on different thiols.[1] This fact suggests that electrochemically active MB molecules are much closer to the Au substrate than the *average* separation determined from the Raman measurements. On the other hand, the relative small value of k for MB immobilized on S can be explained with the different binding of MB to the spacer.

Conclusions

We have presented a detailed Raman study, complemented by STM and electrochemical measurements, of MB immobilized by different spacers on Au electrodes. We have shown that submonolayer sensitivity of MB is accessible by Raman scattering through both electronic resonance and surface plasmon resonance enhancement. These experiments have allowed a precise determination of the MB coverage, irrespective of the electrochemical activity of the involved molecules. The Raman data show that the efficiency for MB immobilization is largest for S and decreasing for the carboxylate thiols and, finally, for the methyl-terminated thiols. The coverage ratio for S/carboxylate/methyl-terminated thiols is ~1/0.4/0.3. In addition, through the analysis of the Raman intensity dependence with the distance to the metal, the SERS data provided important insight into the *average* spatial location of the MB molecules with respect to the Au substrate. As follows from this semiquantitative analysis, we conclude that the average distance of MB to the substrate surface is the smallest for the S spacer, followed by PT and DT, and is largest for MPA and MUA. In addition, consideration of the changes of the Raman spectra of MB on the different spacers gave information on the differing binding and orientation of the molecules. These results indicate that MB on S probably binds through the dimethylamino groups and not through a sulfur−sulfur interaction. Additionally, some differences can be observed from Raman spectra recorded for immobilized MB on methyl- and carboxylate-terminated thiols, suggesting that the orientation of the MB molecules may be different in the two cases.

The presented results allow other interesting conclusions concerning the interaction of methylene blue with organic films. Significant amounts of cationic MB species are able to diffuse into the hydrocarbon chain environment (DT) showing some lipophilic properties, whereas they are readily stopped by negatively charged groups. Most of the molecules immobilized on both methyl- and carboxylate-terminated thiols are electrochemically inactive, suggesting that strong coupling between the Au electrode and the MB molecules is needed for charge transfer. The results are consistent with a small population of electrochemically active MB molecules very close to the Au surface. These active molecules could reach this position driven by their lipophilic (hydrophobic) character through defects at SAMs. The heterogeneous charge transfer rate constant increases with the decrease in electrode/MB distance, but it seems to be also strongly influenced by the MB−SAM interaction.

Acknowledgment. We acknowledge G. Zampieri and H. Ascolani for performing XPS measurements and for enlightening discussions. This work was supported by the Agencia Nacional de Promoción Científica y Tecnológica (PICT 02-11111, PICT 00-8904, RENAMSI and RENAMaN).

References and Notes

(1) Adams, D. M.; Brus, L.; Chidsey, C. E. D.; Creager, S.; Creutz, C.; Kagan, C. R.; Kamat, P. V.; Lieberman, X. M.; Lindsay, O. S.; Marcus, R. A.; Metzger, R. M.; Michel-Beyerle, M. E.; Millar, J. R.; Newton, M. D.; Rolison, D. R.; Sankey, O.; Schanze, K. S.; Yardley, J.; Zhu, S. *J. Phys. Chem. B* **2003**, *107*, 6668−6697, and references therein.

(2) Katz, E.; Shipway, A.; Willnerein, I. In *Handbook of Fuel Cells*; Viesltich, W., Gasteiger, H. A., Lamm, A., Eds.; John Wiley: New York, 2003; Vol. 1, Chapter 21.

(3) Love, J. C.; Estroff, A.; Kriebel, J.; Nuzzo, R.; Whitesides, G. *Chem. Rev.* **2005**, *105*, 1103−1170. Wilbur, L.; Whitesides, G. M.; Nanofabrication. In *Nanotechnology*; Timp, G., Ed.; Springer-Verlag: New York, 1999. Cunningham, A. J. *Introduction to Bioanalytical Sensors*; Wiley-Interscience: New York, 1998.

(4) See, for instance, *Sci. Am.* **2001**, *285* (3); *Science* **2002**, *295*, 2313−2556.

(5) Castner, D. G.; Ratner, B. D. In *Frontiers in Surface and Interface Science*; Duke, C. B., Plummer, E. W., Eds; North-Holland: Amsterdam, 2002.

(6) Pai, E.; Schulz, E. *J. Biol. Chem.* **1983**, *258*, 1752−1757.

(7) Ulman, A. *Chem. Rev.* **1996**, *96*, 1533−1554.

(8) Schreiber, F. *Prog. Surf. Sci.* **2000**, *65*, 151−256.

(9) Vericat, C.; Vela, M. E.; Salvarezza, R. C. *Phys. Chem. Chem. Phys.* **2005**, *7*, 3258−3268.

(10) Benitez, G.; Vericat, C.; Tanco, S.; Remes Lenicov, F.; Castez, M. F.; Vela, M. E.; Salvarezza, R. C. *Langmuir* **2004**, *20*, 5030−5037.

(11) Zharnikov, M.; Frey, S.; Heister, K.; Grunze, M. *Langmuir* **2000**, *16* 2697−2705. Laihi, T.; Leiro, J. A.; Heinonen, M. H.; Mattila, S. S.; Lukkari, J. *J. Electron Spectrosc.* **2005**, *142*, 105−112.

(12) Vericat, C.; Remes Lenicov, F.; Tanco, S.; Andreasen, G.; Vela, M. E.; Salvarezza, R. C. *J. Phys. Chem. B* **2002**, *106*, 9114−9121.

(13) Nelson, D. L.; Cox, M. M.; *Lehninger Principles of Biochemistry*, 3rd ed.; W. H. Freeman & Co: New York, 2000.

(14) Tang, W.; Xu, H.; Kopelman, R.; Philbert, M. A. *Photochem. Photobiol.* **2005**, *81*, 242−249.

(15) Halliwell, B.; Gutteridge, J. M. C. In *Free Radicals in Biology and Medicine*; Oxford University Press: New York, 1989. Johnson, B. E.; Ferguson, J. *Semin. Dermatol.* **1990**, *9*, 39−46.

(16) Jockusch, S.; Lee, D.; Turro, N. J.; Leonard, E. F. *Proc. Natl. Acad. Sci. U.S.A.* **1996**, *93*, 7446−7451.

(17) Palit, D.; Moulik, S. P. *Colloid J.* **2003**, *65*, 350−357.

(18) Colston, J.; Horobin, Rw.; Rashid-Doubell, F.; Pediani, J.; Johal, Kk. *Biotech. Histochem.* **2003**, *78*, 323−332.

(19) Tognalli, N.; Fainstein, A.; Bonazzola, C.; Calvo, E. *J. Chem. Phys.* **2004**, *120*, 1905−1911.

(20) Tognalli, N.; Fainstein, A.; Calvo, E.; Bonazzola, C.; Pietrasanta, L.; Campoy-Quiles, M.; Etchegoin, P. *J. Chem. Phys.* **2005**, *123*, 044707.

(21) Kneipp, K.; Wang, Y.; Kneipp, H.; Perelman, L.; Itzkan, I.; Dasari, R. R.; Feld, M. S. *Phys. Rev. Lett.* **1997**, *78*, 1667−1670.

(22) Nie, S.; Emory, S. R. *Science* **1997**, *275*, 1102−1106.

(23) Maher, R. C.; Cohen, L. F.; Etchegoin, P. *Chem. Phys. Lett.* **2002**, *352*, 378−384.

(24) Dick, L. A.; Haes, A. J.; Van Duyne, R. P. *J. Phys. Chem. B* **2000**, *104*, 11752−11762.

(25) Gao, X.; Davis, J. P.; Weaver, M. J. *J. Phys. Chem.* **1990**, *94*, 6858−6864.

(26) Ye, Q.; Fang, J.; Sun, L. *J. Phys. Chem. B* **1997**, *101*, 8221−8224.

(27) Kennedy, B. J.; Spaeth, S.; Dickey, M.; Carron, K. T. *J. Phys. Chem. B* **1999**, *103*, 3640−3646.

(28) Andreasen, G.; Vela, M. E.; Salvarezza, R. C.; Arvia, A. J. *Langmuir* **1997**, *13*, 6814−6819.

(29) Salvarezza, R. C.; Arvia, A. J. A Modern Approach to Surface Roughness Applied to Electrochemical Systems. In *Modern Aspects of Electrochemistry*; Conway, B. E., Bockris, J. O'M., White, R. E., Eds.; Plenum Press: New York, 1996; Vol. 28, p 289. Alonso, C.; Salvarezza, R. C.; Vara, J. M.; Arvia, A. J.; Vazquez, L.; Bartolomé, A.; Baró, A. M. *J. Electrochem. Soc.* **1990**, *137*, 2161−2175.

(30) Vericat, C.; Andreasen, G.; Vela, M. E.; Salvarezza, R. C. *J. Phys. Chem. B* **2000**, *104*, 302−307.

(31) Vela, M. E.; Martin, H.; Vericat, C.; Andreasen, G.; Hernández Creus, A.; Salvarezza, R. C. *J. Phys. Chem. B* **2000**, *104*, 11878−11882.

(32) Naujok, R. R.; Duevel, R. V.; Corn, R. M. *Langmuir* **1993**, *9*, 1771−1774.

(33) Hutchinson, K.; Hester, R. E.; Albery, W. J.; Hillman, A. R. *J. Chem. Soc., Faraday Trans. 1* **1984**, *80*, 2053−2071.

(34) Dewar, M. J. S.; Zoebisch, E.; Healy, E. F.; Stewart, J. J. P. *J. Am. Chem. Soc.* **1985**, *107*, 3902−3909.

(35) Campbell, D. J.; Higgins, D. A.; Corn, R. M. *J. Phys. Chem.* **1990**, *94*, 3681−3689.

(36) Svetlicic, V.; Zutic, V.; Clavilier, J.; Chevalet, J. *J. Electroanal. Chem.* **1987**, *233*, 199−210.

(37) Nicolai, S. H. A.; Rubim, J. C. *Langmuir* **2003**, *19*, 4291−4294.

(38) Patil, K.; Pawar, R.; Talap, P. *Phys. Chem. Chem. Phys.* **2000**, *2*, 4313−4317.

(39) Laviron, E. *J. Electroanal. Chem.* **1979**, *101*, 19−28.